Probing the $L_\mu - L_\tau$ gauge boson at electron colliders

Yu Zhang,[1,2] Zhuo Yu,[1] Qiang Yang,[3] Mao Song,[2] Gang Li,[2,*] and Ran Ding[2]

[1]*Institutes of Physical Science and Information Technology, Anhui University, Hefei 230601, China*
[2]*School of Physics and Materials Science, Anhui University, Hefei 230601, China*
[3]*Zhejiang Institute of Modern Physics, Department of Physics, Zhejiang University, Hangzhou 310027, China*

(Received 21 September 2020; accepted 16 December 2020; published 6 January 2021)

We investigate the minimal $U(1)_{L_\mu - L_\tau}$ model with extra heavy vectorlike leptons or charged scalars. By studying the kinetic mixing between $U(1)_{L_\mu - L_\tau}$ gauge boson Z' and standard model photon, which is absent at tree level and will arise at one-loop level due to μ, τ, and new heavy charged leptons or scalars, the interesting behavior is shown. It can provide the possibility for visible signatures of new heavy particles. We propose to search for Z' at electron collider experiments, such as Belle II, BESIII, and future Super Tau Charm Factory (STCF), using the monophoton final state. The parameter space of Z' is probed and scanned by its gauge coupling constant $g_{Z'}$ and mass $m_{Z'}$. We find that electron colliders have sensitivity to the previously unexplored parameter space for Z' with MeV–GeV mass. Future STCF experiments with $\sqrt{s} = 2$–7 GeV can exclude the anomalous muon magnetic moment favored area when $m_{Z'} < 5$ GeV with the luminosity of 30 ab^{-1}. For $m_{Z'} < 2m_\mu$, $g_{Z'}$ can be down to 4.2×10^{-5} at 2 GeV STCF.

DOI: 10.1103/PhysRevD.103.015008

I. INTRODUCTION

The standard model (SM) of particle physics is a successful and highly predictive theory of fundamental particles and interactions but fails to explain many phenomena, including neutrino mass, baryon asymmetry of the Universe, and the presence of dark matter and dark energy, among others. It implies that SM is only a low-energy approximation of the more fundamental theory; extensions of SM are strongly required.

Among various extended scenarios beyond SM, new U(1) gauge symmetries are of particular interest since this is one of the minimal extensions of the SM. In particular, the $U(1)_{L_\mu - L_\tau}$ model [1–3], with a $U(1)_{L_\mu - L_\tau}$ extension of SM, gauges the difference of the leptonic muon and tau number and induces a new vector boson Z'. This model has gained a lot of attention, since it can be free from gauge anomaly without any extension of particle content. Moreover, it is potentially able to address important open issues in particle physics, such as the discrepancy in the moun anomalous magnetic moment $(g-2)_\mu$ [4–7], B decay anomalies [8–13], and recent anomalous excess in $K_L \to \pi^0 + \text{INV}$ [14]. Besides, the $U(1)_{L_\mu - L_\tau}$ model has also been discussed in lepton-flavor-violating decay of the Higgs boson [11,15], the neutrino masses and mixing [6,16–18], and dark matter [10,18–26].

Since Z' can directly couple to a muon, related searches for Z' have been performed with the production of $\mu^+\mu^- Z'$ at collider experiments, including *BABAR* [27] and Belle II [28] at electron colliders and CMS [29] at a hadron collider. Subsequently, Z' decaying to muon pair is considered by the *BABAR* and CMS experiments, and invisible decay of Z' is considered at Belle II. Phenomenally, Ref. [30] investigated the sensitivity on Z' at Belle II with the planned target luminosity of 50 ab^{-1} in the channel of $e^+e^- \to \mu^+\mu^- Z', Z' \to \text{INV}$; Refs. [31–34] proposed the search for Z' at Belle II using the monophoton process $e^+e^- \to \gamma Z', Z' \to$ invisible, which depends on the kinetic mixing between the SM photon and Z'; Ref. [35] probes the charged kaon decays $K \to \mu\nu Z'$ at NA62.

In this work, we investigate the $\gamma - Z'$ kinetic mixing in the minimal $U(1)_{L_\mu - L_\tau}$ with extra heavy vectorlike leptons or charged scalars. Then, we propose to search for $L_\mu - L_\tau$ gauge boson Z' at electron collider experiments, such as Belle II, BESIII, and the future Super Tau Charm Factory (STCF), using the monophoton final state. Belle II is an asymmetric detector and located at SuperKEKB, which collides 7 GeV electrons with 4 GeV positrons. SuperKEKB has a largest instantaneous luminosity of 8×10^{35} cm^{-2} s^{-1} [36]. The ambitious goal of SuperKEKB is to accumulate an integrated luminosity of 50 ab^{-1} with 8-year data takings [36]. The BESIII detector is symmetric and operated on the BEPCII with the beam energy ranging from 1.0 to 2.3 GeV and a peak luminosity of 10^{33} cm^{-2} s^{-1}

*lig2008@mail.ustc.edu.cn

[37]. STCF is a proposed symmetric detector experiment which collides electron with a positron in the range of center-of-mass energies from 2.0 to 7.0 GeV with the peak luminosity $\mathcal{O}(10^{35})$ cm^{-2} s^{-1} at 4 GeV [38–40].

The rest of the paper is organized as follows. First, we introduce the $U(1)_{L_\mu - L_\tau}$ models and discuss their phenomenological features. Then, we calculate the cross sections of the signal and the backgrounds and analysis to improve the significance by appropriate event cuts at three different electron colliders operated at the GeV scale: BelleII, BESIII, and STCF. The sensitivities for Z' at these experiments are also investigated. Finally, a short summary and discussions are given.

II. $U(1)_{L_\mu - L_\tau}$ MODELS

A. Minimal $U(1)_{L_\mu - L_\tau}$ model

We extend the SM with a new $U(1)$ gauge symmetry, $U(1)_{L_\mu - L_\tau}$, where leptons of the second and third generations couple to the additional $U(1)_{L_\mu - L_\tau}$ gauge boson Z' with equal and opposite charge. The new leptonic gauge interactions can be given as

$$\mathcal{L}_{\rm int} = g_{Z'}(\bar{\mu}\gamma^\mu\mu - \bar{\tau}\gamma^\mu\tau + \bar{\nu}_\mu\gamma^\mu P_L\nu_\mu - \bar{\nu}_\tau\gamma^\mu P_L\nu_\tau)Z'_\mu, \quad (1)$$

where $g_{Z'}$ is gauge coupling constant.

In the minimal $U(1)_{L_\mu - L_\tau}$ model, the kinetic mixing between the Z' and photon is absent at the tree level. Nevertheless, because μ and τ are both charged under the electromagnetic $U(1)$ and $U(1)_{L_\mu - L_\tau}$, there exists an unavoidable kinetic mixing at one-loop level, which can appear as [32]

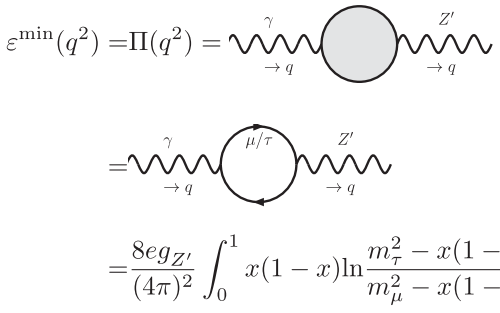

$$= \frac{8eg_{Z'}}{(4\pi)^2}\int_0^1 x(1-x)\ln\frac{m_\tau^2 - x(1-x)q^2}{m_\mu^2 - x(1-x)q^2}\,dx. \quad (2)$$

Here, e is the electromagnetic charge, m_τ and m_μ are the masses of tau and muon leptons, and q is the transferred momentum.

For large momentum transfer $q^2 \gg m_\tau^2$, this mixing is power suppressed by $1/q^2$, whereas for low momentum transfer $q^2 \sim 0 \ll m_\mu^2$, the mixing tends to be a constant,

$$\varepsilon^{\rm min}(0) = \Pi(0) = \frac{eg_{Z'}}{6\pi^2}\ln\frac{m_\tau}{m_\mu}, \quad (3)$$

which seems like the dark photon model.

B. $U(1)_{L_\mu - L_\tau}$ model with extra heavy vectorlike leptons

We add two extra singlet vectorlike leptons (L_1, L_2) in the $U(1)_{L_\mu - L_\tau}$ extension of the SM, which are charged under $U(1)_{L_\mu - L_\tau}$ opposite in sign similar to the μ and τ and have electric charge of e [33]. Since we mainly focus on the gauge kinetic mixing, we will not provide much details of the model here. In this model, due to the leptons inside the loop, the kinetic mixing of γ and Z' can be derived as

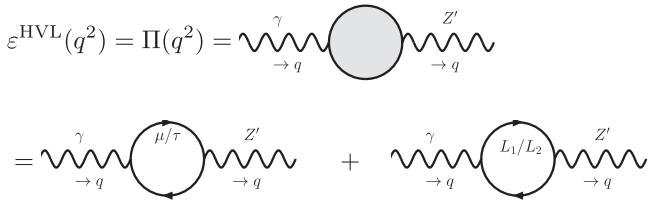

$$= \frac{8eg'}{(4\pi)^2}\int_0^1 x(1-x)\Big[\ln\frac{m_\tau^2 - x(1-x)q^2}{m_\mu^2 - x(1-x)q^2} + \ln\frac{m_{L_2}^2 - x(1-x)q^2}{m_{L_1}^2 - x(1-x)q^2}\Big]\,dx. \quad (4)$$

Here, m_{L_1} and m_{L_2} are the masses of L_1 and L_2. When the momentum transfer $q^2 \ll m_{L_1/L_2}$, which is considered in this work, the mixing can be simplified as

$$\varepsilon^{\rm HVL}(q^2, r) = \varepsilon^{\rm min}(q^2) + \frac{eg_{Z'}}{6\pi^2}\ln r, \quad (5)$$

where $r = m_{L_2}/m_{L_1}$ is the mass ratio of L_1 and L_2.

C. $U(1)_{L_\mu - L_\tau}$ model with extra heavy charged scalars

In the $U(1)_{L_\mu - L_\tau}$ extension of the SM, we add two extra scalars (S_1, S_2) with electric charge of e and charged under $U(1)_{L_\mu - L_\tau}$ opposite in sign [34]. Similarly, due to charged leptons and extra scalars contributions induced at one-loop level, the $\gamma - Z'$ kinetic mixing can be given as

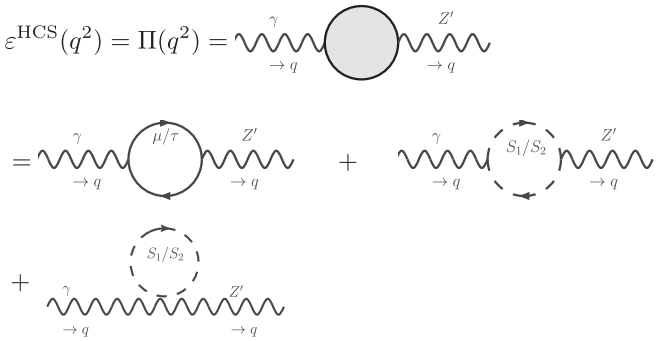

$$= \frac{8eg'}{(4\pi)^2}\int_0^1 dx\; x(1-x)\ln\frac{m_\tau^2 - x(1-x)q^2}{m_\mu^2 - x(1-x)q^2} + \frac{2eg'}{(4\pi)^2}\int_0^1 dx\;(1-2x)^2\ln\frac{m_{S_2}^2 - x(1-x)q^2}{m_{S_1}^2 - x(1-x)q^2}\;. \quad (6)$$

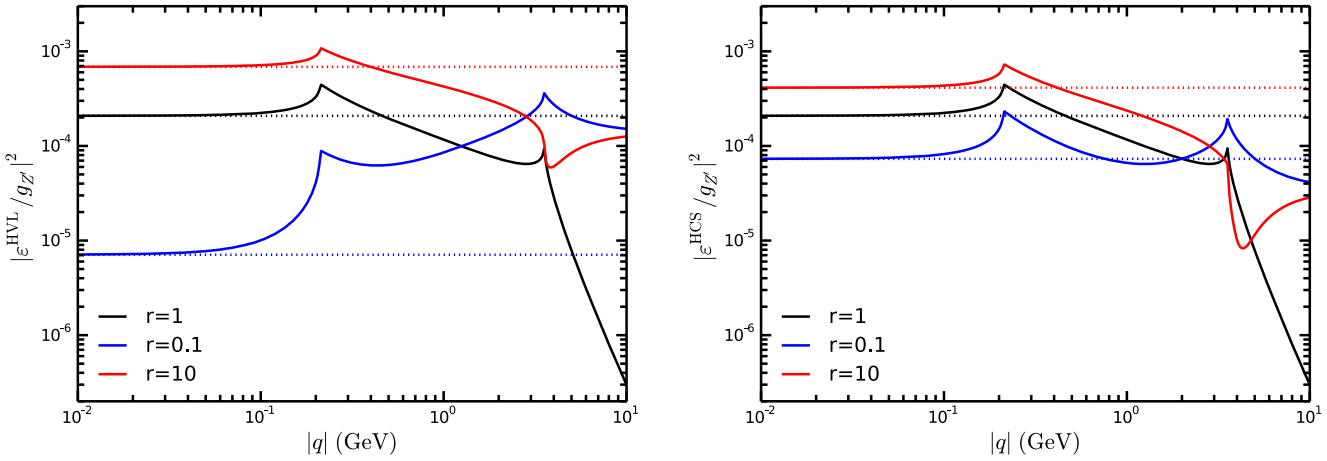

FIG. 1. The square of the kinetic mixing $|\varepsilon/g_{Z'}|^2$ as a function of the momentum transfer $|q|$ with the mass ratio $r = 0.1$, 1, and 10 for the $U(1)_{L_\mu - L_\tau}$ model with extra heavy vectorlike leptons (left) or charged scalars (right). As a comparison, the cases with zero momentum transfer $(q^2 = 0)$, are also shown by the horizontal dotted lines.

Here, m_{S_1} and m_{S_2} are the masses of extra charged scalars (S_1 and S_2). We mainly focus on the gauge kinetic mixing; thus, many details of the model are not provided here.

In this work, we consider the momentum transfer always $q^2 \ll m_{S_1/S_2}$; thus, the mixing can be also written as

$$\varepsilon^{\rm HCS}(q^2, r) = \varepsilon^{\rm min}(q^2) + \frac{e g_{Z'}}{24\pi^2} \ln r, \tag{7}$$

where $r = m_{S_2}/m_{S_1}$ is the mass ratio of S_2 and S_1.

In Fig. 1, we present the square of the kinetic mixing $|\varepsilon^{\rm HVL,HCS}/g_{Z'}|^2$ as a function of the momentum transfer $|q|$ with $r = 0.1$, 1, and 10. As a comparison, the cases with zero momentum transfer $(q^2 = 0)$, are also shown by the horizontal dotted lines. When $r = 1$, the contribution for the kinetic mixing due to additional leptons or scalars vanishes, and the results will become the same as those in the minimal $U(1)_{L_\mu - L_\tau}$ model, i.e., $\varepsilon^{\rm HVL}(q^2, 1) = \varepsilon^{\rm HCS}(q^2, 1) = \varepsilon^{\rm min}(q^2)$. In the minimal $U(1)_{L_\mu - L_\tau}$ model, $|\varepsilon/g_{Z'}|^2$ has two peaks at the position of $|q| = m_\mu$ and $|q| = m_\tau$ and drops quickly with the increment of $|q|$ when $|q| > m_\tau$. This feature distinguishes the phenomenology of the $U(1)_{L_\mu - L_\tau}$ model from the dark photon models with a constant value of the kinetic mixing.

We also present the dependence of the kinetic mixing ratio $R = |\varepsilon^{\rm HVL/HCS}|^2/|\varepsilon^{\rm min}|^2$ between the $U(1)_{L_\mu - L_\tau}$ model with two singlet vectorlike leptons or with two charged scalars and the minimal $U(1)_{L_\mu - L_\tau}$ model on the mass ratio r in Fig. 2. There, we consider five typical momentum transfers $|q| = 0.1$ GeV, 1 GeV, 10 GeV, $2m_\mu$, $2m_\tau$. It can be seen that the additional lepton or scalar contributions could be significant, and the results are distinctly different from those of the minimal $U(1)_{L_\mu - L_\tau}$ model. Though the additional leptons and scalars cannot be detected directly due to their heavy mass, they can provide significant contributions to the kinetic mixing.

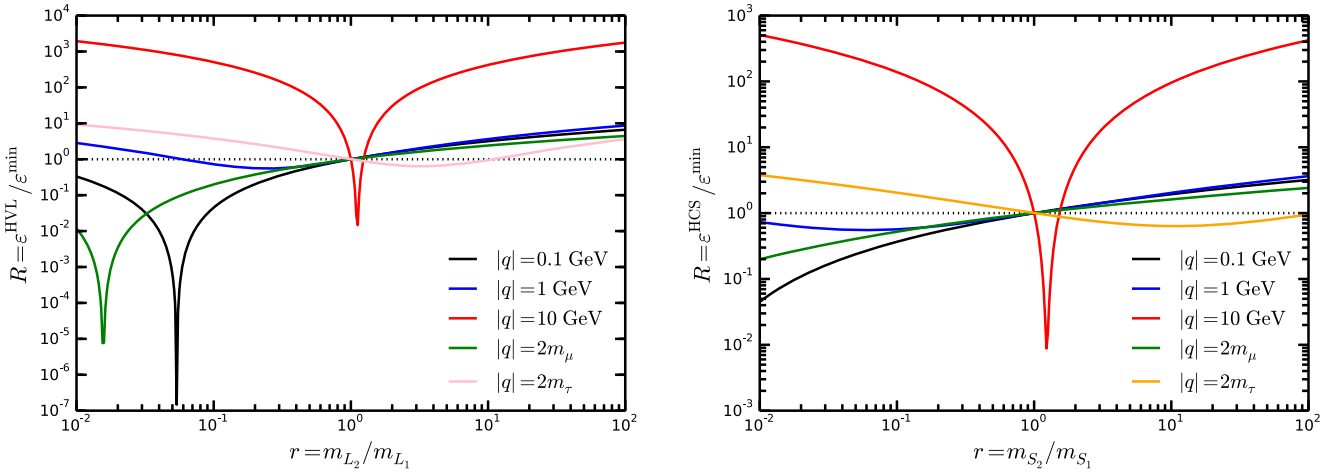

FIG. 2. The ratio $R = |\varepsilon^{\rm TSL,SUSY}|^2/|\varepsilon^{\rm min}|^2$ of the kinetic mixing between $U(1)_{L_\mu - L_\tau}$ model with extra heavy vectorlike leptons (left) or charged scalars (right) and the minimal $U(1)_{L_\mu - L_\tau}$ model as the function of mass ratio r with momentum transfer $|q| =$ 0.1 GeV, 1 GeV, 10 GeV, $2m_\mu$, $2m_\tau$.

D. Decay modes of Z'

Since the Z' direct couples with the leptons of second and third generations, it can decay into a pair of neutrinos and also may decay into muon and tau leptons if kinematically allowed. In addition, since Z' provides possible scenarios of dark matter, there can be the channel $Z' \to \chi\bar{\chi}$. The decay widths of Z' are given by

$$\Gamma(Z' \to \nu_\ell \bar{\nu_\ell}) = \frac{g_{Z'}^2}{24\pi} m_{Z'}, \tag{8}$$

$$\Gamma(Z' \to \ell^+\ell^-) = \frac{g_{Z'}^2}{12\pi} m_{Z'} \left[1 + \frac{2m_\ell^2}{m_{Z'}^2}\right] \sqrt{1 - \frac{4m_\ell^2}{m_{Z'}^2}}, \tag{9}$$

$$\Gamma(Z' \to \chi\bar{\chi}) = \frac{g_D^2}{12\pi} m_{Z'} \left[1 + \frac{2m_\chi^2}{m_{Z'}^2}\right] \sqrt{1 - \frac{4m_\chi^2}{m_{Z'}^2}}, \tag{10}$$

where $\ell = \{\mu, \tau\}$, g_D is the coupling constant of the Z' with dark matter, and $g_D \gg g_{Z'}$ is assumed. We ignore the channel $Z' \to e^+e^-$ since it is suppressed by the kinetic mixing. Since neutrinos and dark matter are invisible at particle detectors, we take the Z' invisible decay as $\Gamma(Z' \to \mathrm{INV}) = \Gamma(Z' \to \nu\bar{\nu}) + \Gamma(Z' \to \chi\bar{\chi})$, whose decay ratio can be expressed as

$$\mathrm{Br}(Z' \to \mathrm{INV}) = \begin{cases} 1, & (m_{Z'} < 2m_\mu \quad \text{or} \quad m_{Z'} > 2m_\chi), \\ \frac{\Gamma(Z' \to \nu\bar{\nu})}{\sum_{f=\nu,\mu} \Gamma(Z' \to f\bar{f})}, & (2m_\mu < m_{Z'} < 2m_\tau \quad \text{and} \quad m_{Z'} < 2m_\chi), \\ \frac{\Gamma(Z' \to \nu\bar{\nu})}{\sum_{f=\nu,\mu,\tau} \Gamma(Z' \to f\bar{f})}, & (2m_\tau < m_{Z'} \quad \text{and} \quad m_{Z'} < 2m_\chi). \end{cases} \tag{11}$$

III. EXISTING CONSTRAINTS

In this section, we summarize the existing constraints relevant to the parameter regions we are interested for the minimal $U(1)_{L_\mu - L_\tau}$ model from various experiments as follows:

(i) *Muon anomalous magnetic moment.*—The significant discrepancy between the experimental measurement and the SM prediction in the magnetic moment of the muon remains one of the largest anomalies in particle physics [41],

$$\Delta a_\mu^{Z'} \equiv a_\mu^{\mathrm{exp}} - a_\mu^{\mathrm{SM}} = (261 \pm 61_{\mathrm{exp}} \pm 48_{\mathrm{the}}) \times 10^{-11}, \tag{12}$$

where the errors are from experiment and theory prediction, respectively. We require the contribution in Eq. (12) to be within 2σ, which leads to

$$103 \lesssim \Delta a_\mu^{Z'} \times 10^{11} \lesssim 420. \tag{13}$$

The minimal $U(1)_{L_\mu - L_\tau}$ model was first introduced to address the discrepancy, which can provide a new interaction with muons. An extra contribution to a_μ arises solely from a one-loop diagram involving Z', which can be giving by

$$a_\mu^{Z'} = \frac{g_{Z'}^2}{8\pi^2} \int_0^1 \frac{2m_\mu^2 x^2(1-x)}{x^2 m_\mu^2 + (1-x) m_{Z'}^2} dx. \tag{14}$$

The parameter region on which the Z' contribution in the minimal $L_\mu - L_\tau$ model resolves the discrepancy in the muon anomalous magnetic moment at 2σ is indicated with the red band in Fig. 3.

(ii) *Neutrino trident production.*—The neutrino trident production is a muon neutrino scattering off the

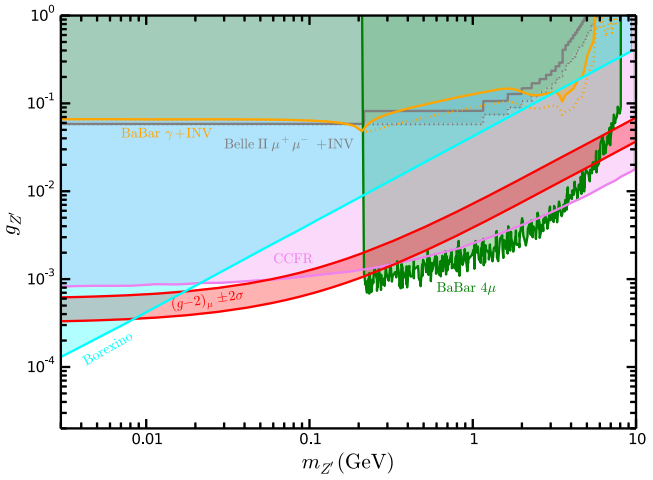

FIG. 3. Summary for the $m_{Z'} - g_{Z'}$ parameter space of the minimal $U(1)_{L_\mu - L_\tau}$ model, where Z' has no additional decay channel to dark sector. The shaded regions show the existing bounds excluded by CCFR experiment in neutrino trident production [42]; by the Borexino detector in neutrino-electron scattering [48]; by the *BABAR* in the reactions $e^+e^- \to \mu^+\mu^- Z', Z' \to \mu^+\mu^-$ with 514 fb^{-1} data [27] and $e^+e^- \to \gamma Z', Z' \to$ INV with 53 fb^{-1} data [50]; and by Belle II in the process $e^+e^- \to \mu^+\mu^- Z', Z' \to$ INV with 276 pb^{-1} data [28]. The dotted lines indicate $\mathrm{BR}(Z' \to \mathrm{INV}) \simeq 1$ cases. The red band indicates the allowed region at 2σ from the experimental measurements of muon magnetic momentum.

Coulomb field of a target nucleus (N), producing two muons in the final state, $\nu N \to \nu N \mu^+ \mu^-$. Besides the SM Z boson, in the $U(1)_{L_\mu - L_\tau}$ model, the Z' boson can also contribute to this process, which can offer a sensitive search for the light Z' boson [42,43]. The measurements for the cross section have been reported by CCFR, which obtained the result $\sigma_{\rm CCFR}/\sigma_{\rm SM} = 0.82 \pm 0.28$. The bound is depicted in Fig. 3 and taken from Ref. [42].

(iii) *Neutrino-electron scattering*.—The neutrino-electron elastic scattering processes can probe $U(1)_{L_\mu - L_\tau}$ gauge boson, since the $U(1)_{L_\mu - L_\tau}$ gauge boson can contribute through the kinetic mixing. The most stringent constraints come from the Borexino solar neutrino experiment. Limits for the $U(1)_{L_\mu - L_\tau}$ gauge boson have been derived in Refs. [32,44,45] by converting existing bounds on $U(1)_{B-L}$ models [46] using earlier Borexino ^{7}Be data [47]. The bounds are updated in Ref. [48] using the recently released Borexino measurement of ^{7}Be neutrinos [49]. We show them in Fig. 3.

(iv) *Z' production associated with muon pair*.—Via the direct coupling to μ, Z' can be produced at e^+e^- colliders in the process $e^+e^- \to \mu^+\mu^- Z'$. The *BABAR* experiment has reported the bounds using 514 fb^{-1} data collected in the reaction $e^+e^- \to \mu^+\mu^- Z', Z' \to \mu^+\mu^-$ for $m_{Z'} > 2m_\mu$ [27]. Recently, the Belle II experiment performed the first searches for the invisible decay of a Z' in the process $e^+e^- \to \mu^+\mu^- Z', Z' \to$ INV using 276 pb^{-1} collected [28], which can touch the region of $m_{Z'} < 2m_\mu$.

(v) *Z' production associated with SM photon*.—At e^+e^- colliders, the Z' boson can also be produced associated with SM photon via the kinetic mixing in the process $e^+e^- \to \gamma Z'$ [50]. The search for invisible decays of the dark photon has been preformed by the *BABAR* experiment using the single-photon events with 53 fb^{-1} data. We translate the constraints for the dark photon to the $U(1)_{L_\mu - L_\tau}$ gauge boson Z' using

$$\varepsilon_{\rm DP}^2 \to |\varepsilon|^2 {\rm Br}(Z' \to {\rm INV}), \tag{15}$$

where $\varepsilon_{\rm DP}$ is the photon and dark photon kinetic mixing parameter in the dark photon model and ε is the $\gamma - Z'$ kinetic mixing in the $U(1)_{L_\mu - L_\tau}$ model.

In Fig. 3, we assume Z' does not decay into dark sector, i.e., $\Gamma(Z' \to {\rm INV}) = \Gamma(Z' \to \nu\bar{\nu})$. The ${\rm BR}(Z' \to {\rm INV}) \simeq 1$ cases are also shown as a dotted line for a visual display. Taking the constraints above into account, a narrow window of the $m_{Z'} - g_{Z'}$ parameter region in the minimal $U(1)_{L_\mu - L_\tau}$ model desired by the muon anomalous magnetic moment,

$$10\,{\rm MeV} \lesssim M_{Z'} \lesssim 210\,{\rm MeV}, \quad 4 \times 10^{-4} \lesssim g_X \lesssim 10^{-3}, \tag{16}$$

is still allowed.

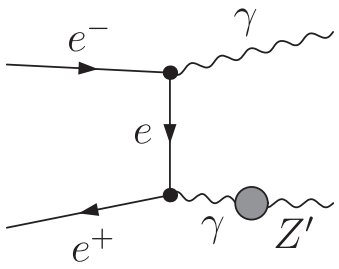

FIG. 4. The Feynman diagrams for the production of an on-shell Z' and a photon.

IV. SEARCHING FOR $U(1)_{L_\mu - L_\tau}$ GAUGE BOSON AT ELECTRON COLLIDERS

At the electron colliders, the production of Z' can be associated with a SM photon through the kinetic mixing in the process $e^+e^- \to \gamma Z'$, whose diagrams are shown in Fig. 4. Subsequently, the produced Z' boson can decay into charged leptons, a pair of neutrinos, or light dark matter. In this paper, we focus on the Z' invisible decay channel $Z' \to$ INV, including $Z' \to \nu\bar{\nu}$ and $Z' \to \chi\bar{\chi}$, to probe Z' boson via the monophoton searches $e^+e^- \to \gamma Z' \to \gamma +$ INV at electron colliders. We assume that the decay width of the Z' is negligible compared to the experimental resolution, which justifies the use of the narrow width approximation.

In the monophoton signature at electron colliders, the major backgrounds (BGs) from SM contain two types: irreducible and reducible BG. The irreducible monophoton BG comes from the process $e^+e^- \to \nu\bar{\nu}\gamma$, where ν is the three neutrinos. The reducible monophoton BG arises from the electromagnetic processes $e^+e^- \to \gamma + \not{X}$, where $\not{X}$ denotes other visible particles which are, however, undetectable due to the limitations of the detector acceptance. We discuss the reducible BG in detail later for each experiment, since it strongly depends on the angular coverage of the detectors.

The differential cross section for an on-shell Z' and a photon production process $e^+e^- \to \gamma Z'$ is [51]

$$\frac{d\sigma_{\gamma Z'}}{dz_\gamma} = \frac{2\pi\alpha^2 |\varepsilon(m_{Z'}^2)|^2}{s}\left(1 - \frac{m_{Z'}^2}{s}\right)\frac{1 + z_\gamma^2 + \frac{4sm_{Z'}^2}{(s-m_{Z'}^2)^2}}{(1+z_\gamma)(1-z_\gamma)}, \tag{17}$$

where α is the fine structure constant, $z_\gamma \equiv \cos\theta_\gamma$, with θ_γ being the relative angle between the electron beam axis and the photon momentum in the center-of-mass (CM) frame, s is the square of the CM energy, and $m_{Z'}$ is the mass of the $U(1)_{L_\mu - L_\tau}$ gauge boson. The photon energy E_γ in the CM frame is related to the Z' mass as

$$E_\gamma = \frac{s - m_{Z'}^2}{2\sqrt{s}}. \tag{18}$$

The cross section after integrating the polar angle θ_γ is given as [51]

$$\sigma_{\gamma Z'} = \frac{2\pi\alpha^2|\varepsilon(m_{Z'}^2)|^2}{s}\left(1-\frac{m_{Z'}^2}{s}\right) \times\left[\left(1+\frac{2sm_{Z'}^2}{(s-m_{Z'}^2)^2}\right)\mathcal{Z}-z_\gamma^{\max}+z_\gamma^{\min}\right], \quad (19)$$

where

$$\mathcal{Z}=\ln\frac{(1+z_\gamma^{\max})(1-z_\gamma^{\min})}{(1-z_\gamma^{\max})(1+z_\gamma^{\min})}. \quad (20)$$

V. BELLE II

At Belle II, photons and electrons can be detected in the Electromagnetic Calorimeter (ECL), which is made up of three segments: forward end cap with $12.4° < \theta < 31.4°$, barrel with $32.2° < \theta < 128.7°$, and backward end cap $130.7° < \theta < 155.1°$ in the laboratory frame [36]. At Belle II, the reducible BG for the monophoton signature consists of two major parts: one is mainly due to the lack of polar angle coverage of the ECL near the beam directions, which is referred to as the "bBG"; the other one is mainly due to the gaps between the three segments in the ECL detector, which is referred to as the "gBG."

The bBG comes from the electromagnetic processes $e^+e^-\to\gamma+\not{X}$, mainly including $e^+e^-\to\gamma\gamma\gamma$ and $e^+e^-\to\ell^+\ell^-\gamma$, where all the other final state particles except the detected photon are emitted along the beam directions with $\theta > 155.1°$ or $\theta < 12.4°$ in the laboratory frame. At Belle II, we adopt the detector cuts for the final detected photon (hereafter the "preselection cuts"): $12.4° < \theta_\gamma < 155.1°$ in the laboratory frame.

In Fig. 5, we show the production rates of the process $e^+e^-\to\gamma Z'$ in $U(1)_{L_\mu-L_\tau}$ models after the preselection cuts for the photon at Belle II with $\sqrt{s}=10.58$ GeV. The dotted lines correspond to the case of constant $\varepsilon(q^2=0)$, which are shown as a comparison. We can see that, with constant $\varepsilon(q^2=0)$, the cross sections all increase with the increment of the mass of Z'. In the minimal $U(1)_{L_\mu-L_\tau}$ model, the production rates for the process $e^+e^-\to\gamma Z'$ at Belle II exist two peaks at the positions of m_μ and m_τ when $m_{Z'} < 8.5$ GeV, and a valley at the tail of the plotted region.

For the Belle II detector, which is asymmetric, the maximum energy of the monophoton events in the bBG in the CM frame, E_γ^m, is given by [52] (if not exceeding $\sqrt{s}/2$)

$$E_\gamma^m(\theta_\gamma)=\frac{\sqrt{s}(A\cos\theta_1-\sin\theta_1)}{A(\cos\theta_1-\cos\theta_\gamma)-(\sin\theta_\gamma+\sin\theta_1)}, \quad (21)$$

where all angles are given in the CM frame, and $A=(\sin\theta_1-\sin\theta_2)/(\cos\theta_1-\cos\theta_2)$, with θ_1 and θ_2 being the polar angles corresponding to the edges of the ECL detector. To remove the above bBG, we use the detector cut $E_\gamma > E_\gamma^m$ (hereafter the "bBG cuts") for the final monophoton.

The gBG for the monophoton signature has been simulated in the Ref. [36] to search for dark photons decaying into light dark matter. The projected upper limits on the kinetic mixing of dark photon and SM photon ε for a 20 fb^{-1} Belle II dataset are present there. The constraint for the kinetic mixing between the $U(1)_{L_\mu-L_\tau}$ gauge boson and SM photon ε can be translated from the dark photon using Eq. (15). In order to obtain the expected sensitivity $\mathcal{S}(g_{Z'})$ at Belle II with the planned target integrated luminosity 50 ab^{-1}, we rescale the current sensitivity by $\mathcal{S}(g_{Z'})\propto\sqrt[4]{\mathcal{L}}$. Then, the corresponding constraint based on the simulation in Ref. [36] from 20 fb^{-1} to 50 ab^{-1} can be simply projected by a factor of $\sqrt[4]{\frac{50/\text{ab}}{20/\text{fb}}}$, which is present in Fig. 6, and the invisible decay ratio $\text{Br}(Z'\to\text{INV})\simeq 1$ is assumed. It is shown that the sensitivity for $g_{Z'}$ at Belle II

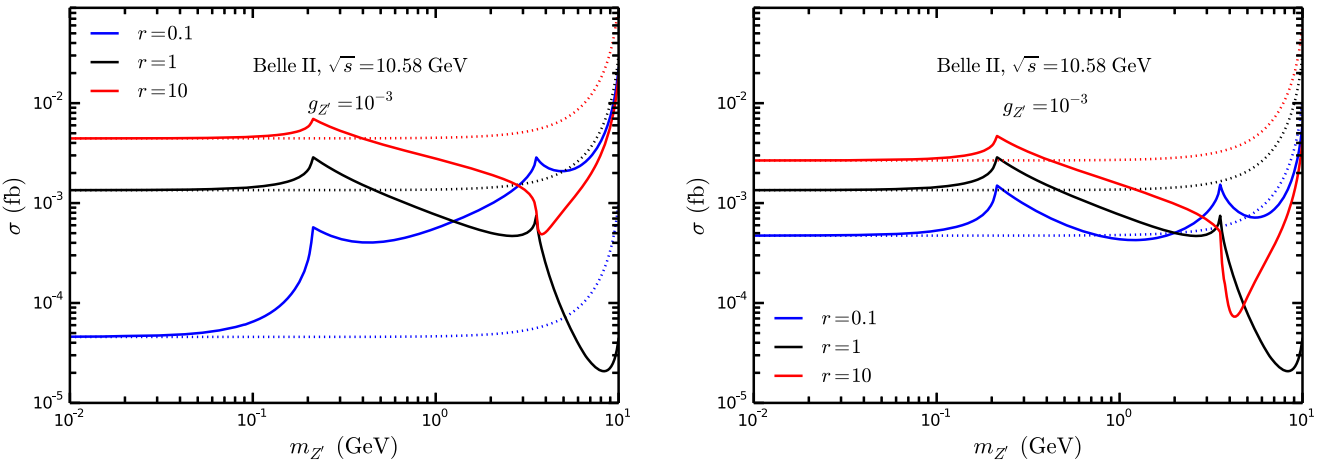

FIG. 5. The cross sections of the process $e^+e^-\to\gamma Z'$ at Belle II with $\sqrt{s}=10.58$ GeV after the preselection cuts for the $L_\mu-L_\tau$ model with extra heavy vectorlike leptons (left) or charged scalars (right). As a comparison, the dotted lines correspond to the case of constant $\varepsilon(q^2=0)$.

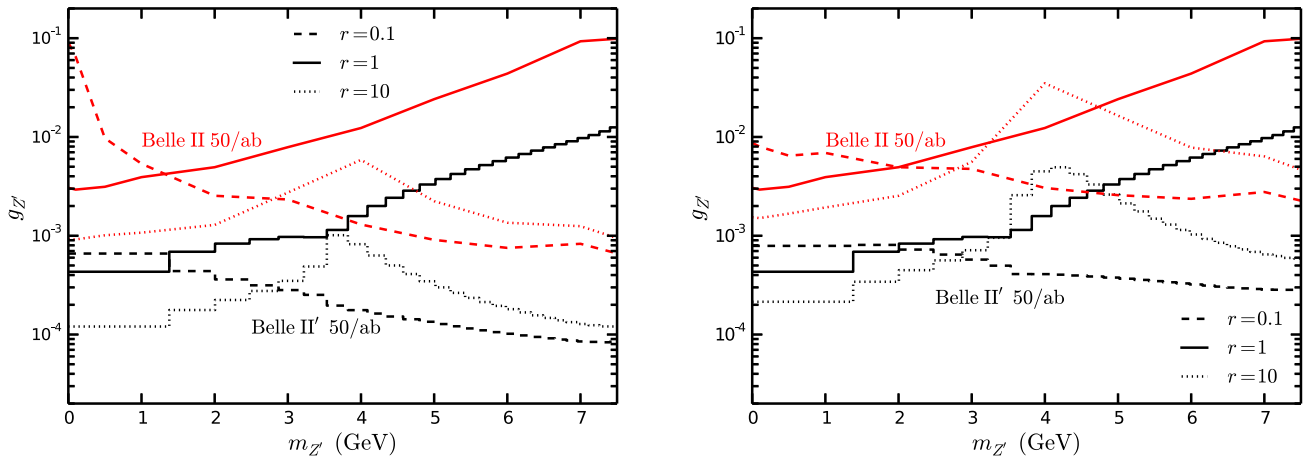

FIG. 6. Sensitivity limit for $g_{Z'}$ at Belle II experiment with 50 ab^{-1} to search for a dark photon decaying into light dark matter based on the simulation in Ref. [36], labeled as "Belle II," red color. The expected 95% C.L. exclusion limits on $g_{Z'}$ via monophoton searches at 50 ab^{-1} Belle II with gBG omitted after the optimized cut, labeled as Belle II′, black color. For the $L_\mu - L_\tau$ model with extra heavy vectorlike leptons (left) or charged scalars (right) in the cases of $r = 0.1$ (dashed), 1 (solid), and 10 (dotted).

experiment with 50 ab^{-1} via monophoton searches is expected to be worse in the minimal $U(1)_{L_\mu - L_\tau}$ model with the increment of $m_{Z'}$, while becoming better with extra heavy vectorlike leptons (charged scalars) in the case of $r = 0.1$ when $m_{Z'} < 7$ GeV. With $r = 10$ in the $U(1)_{L_\mu - L_\tau}$ model with extra heavy leptons (scalars), expected $g_{Z'}$ sensitivity gets improved when $m_{Z'} \gtrsim 4$ GeV and then gets worse.

We further carry out an analysis without gBG taken into account, to compare with other experiments in which detailed simulations with gBG are not available. We use the "bBG cuts" to remove the reducible BG events; the BG events that survived the "bBG cuts" come from irreducible BGs, if gBG is not considered. Since the energy of the final photon in the signal process is related to $m_{Z'}$, in addiction to the bBG cuts, we select the final photon in the energy window of $|E_\gamma - (s - m_{Z'}^2)/(2\sqrt{s})| < \sigma_E/2$ (hereafter the "optimized cut") to enhance the discovery sensitivity, where σ_E is the detector energy resolution for the photon. At Belle II, $\sigma_E/E = 4\%(1.6\%)$ at 0.1 (8) GeV [36] and we take $\sigma_E = 128$ MeV conservatively. In Fig. 6, we present the expected 95% confidence level (C.L.) exclusion limits on $g_{Z'}$ by considering the irreducible BG only after the optimized cut, which is labeled as Belle II′. We define $\chi^2(\varepsilon) \equiv S^2/(S + B)$ [53], where S (B) is the number of events in the signal (BG) processes. The 95% C.L. upper bound on $g_{Z'}$ is obtained by solving $\chi^2(\epsilon_{95}) - \chi^2(0) = 2.71$ and assuming photon detection efficiency as 95% [36]. One can see that if we do not consider the gBG and apply the optimized cut the Belle II experiment with 50 ab^{-1} via monophoton searches is expected to be sensitive to the parameter region with $m_{Z'} \lesssim 1.2$ GeV and $g_{Z'} \gtrsim 4 \times 10^{-4}$ in the minimal $L_\mu - L_\tau$ model, which can be improved by almost 1 order of magnitude compared with considering the gBG.

VI. BESIII AND STCF

At BESIII and STCF, for the final state photons, we adopt the preselection cuts by the BESIII Collaboration [54]: $E_\gamma > 25$ MeV with $|\cos\theta| < 0.8$ or $E_\gamma > 50$ MeV with $0.86 < |\cos\theta| < 0.92$. In Fig. 7, we present the cross section of the process $e^+e^- \to \gamma Z'$ at BESIII and STCF with $\sqrt{s} = 4$ GeV in $U(1)_{L_\mu - L_\tau}$ models after the preselection cuts. As a comparison, the dotted lines correspond to the case of constant $\varepsilon(q^2 = 0)$. One can see that the cross section always increases for larger $m_{Z'}$ in $U(1)_{L_\mu - L_\tau}$ models with extra heavy leptons or scalars in the case of $r = 0.1$, while there is a twist near $m_{Z'} = 2m_\tau$ in the case of $r = 1$ and $r = 10$.

At BESIII and STCF, which are symmetric, the maximum energy of the monophoton events in the bBG in the CM frame, E_γ^m, is given by [55]

$$E_\gamma^m(\theta_\gamma) = \sqrt{s}\left(\frac{\sin\theta_\gamma}{\sin\theta_b}\right)^{-1}, \tag{22}$$

where $\cos\theta_b$ is the polar angle corresponding to the edge of the detector. Taking into account the coverage of main drift chamber (MDC), electromagnetic calorimeter (EMC), and time-of-flight (TOF), we have $\cos\theta_b = 0.95$ at the BESIII [56]. We further demand $E_\gamma > E_\gamma^m$ for the final monophoton to remove the reducible BG (hereafter the *bBG cuts*).

At BESIII, the photon energy resolution of the EMC $\sigma_E/E = 2.3\%/\sqrt{E/\text{GeV}} \oplus 1\%$ [37], and we take $\sigma_E =$ 40 MeV for all energy conservatively. At the BESIII, photon reconstruction efficiencies are all more than 99% [57], and we assume them to be 100% in our paper. For the EMC at STCF, we assume the same energy resolution and reconstruction efficiencies with BESIII to present a preliminary projection limit because of the similarity of the two experiments. We take $\sigma_E = 25(40, 50)$ MeV for $\sqrt{s} = 2, (4, 7)$ GeV. In addition to the bBG cuts, we select

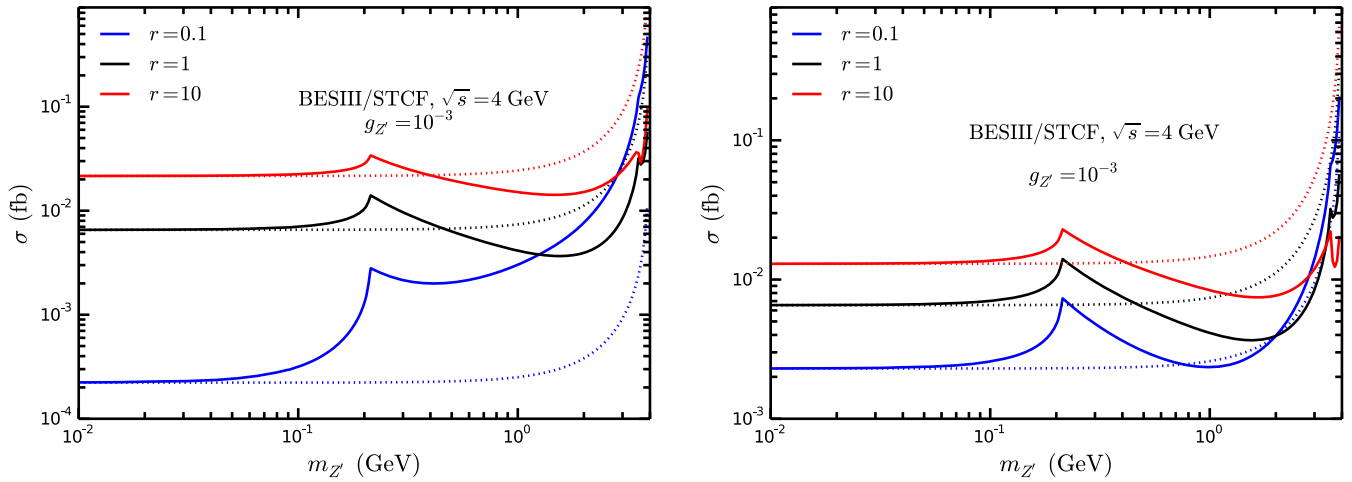

FIG. 7. The cross sections of the process $e^+e^- \to \gamma Z'$ at BESIII or STCF with $\sqrt{s} = 10.58$ GeV after the preselection cuts for the $L_\mu - L_\tau$ model with extra heavy vectorlike leptons (left) or charged scalars (right). As a comparison, the dotted lines correspond to the case of constant $\varepsilon(q^2 = 0)$.

final photon in the energy window of $|E_\gamma - (s - m_{Z'}^2)/(2\sqrt{s})| < \sigma_E/2$ (hereafter the *optimized cut*) to enhance the discovery sensitivity.

At BESIII, since 2012, the monophoton trigger has been implemented, and the corresponding data luminosity reach about 14 fb^{-1} with the CM energy from 2.125 to 4.6 GeV [58]. We define $\chi^2_{\rm tot}(\varepsilon) = \sum_i \chi^2_i(\varepsilon)$, where $\chi^2_i(\varepsilon) \equiv S_i^2/(S_i + B_i)$ for each BESIII colliding energy. The 95% C.L. upper bound on $g_{Z'}$ from BESIII is obtained by demanding $\chi^2_{\rm tot}(\varepsilon_{95}) - \chi^2_{\rm tot}(0) = 2.71$. In Fig. 8, we present the corresponding results for the $U(1)_{L_\mu - L_\tau}$ models with extra vectorlike leptons and charged scalars in cases of $r = 0.1, 1, 10$ via monophoton searches at BESIII with 14 fb^{-1} and at 4 GeV STCF with 30 ab^{-1}, respectively. The invisible decay ratio of Z' is assumed to be 1. The constraints on $g_{Z'}$ get looser with the increment of $m_{Z'}$ for both considered models in cases of $r = 1, 10$ at BESIII and 4 GeV STCF, while they get tighter in cases of $r = 0.1$ for the $U(1)_{L_\mu - L_\tau}$ models with extra leptons (scalars) when $m_{Z'} \lesssim 2.7$ GeV (1.0 GeV $\lesssim m_{Z'} \lesssim 2.7$ GeV) at 4 GeV STCF.

VII. RESULTS

Figure 9 summarizes the sensitivity on gauge coupling $g_{Z'}$ in the minimal $L_\mu - L_\tau$ model from electron colliders, including Belle II, BESII, and STCF. The solid lines indicate the case in which Z' cannot decay into dark matter, i.e., $\mathrm{Br}(Z' \to \mathrm{INV}) = \mathrm{Br}(Z' \to \nu\bar{\nu})$, and the dotted lines indicate the $\mathrm{Br}(Z' \to \mathrm{INV}) \simeq 1$ case. The existing constraints are also presented in the shaded region, and the summary for these limits from different experiments can be found in Fig. 3. The red band shows the region that could explain the muon

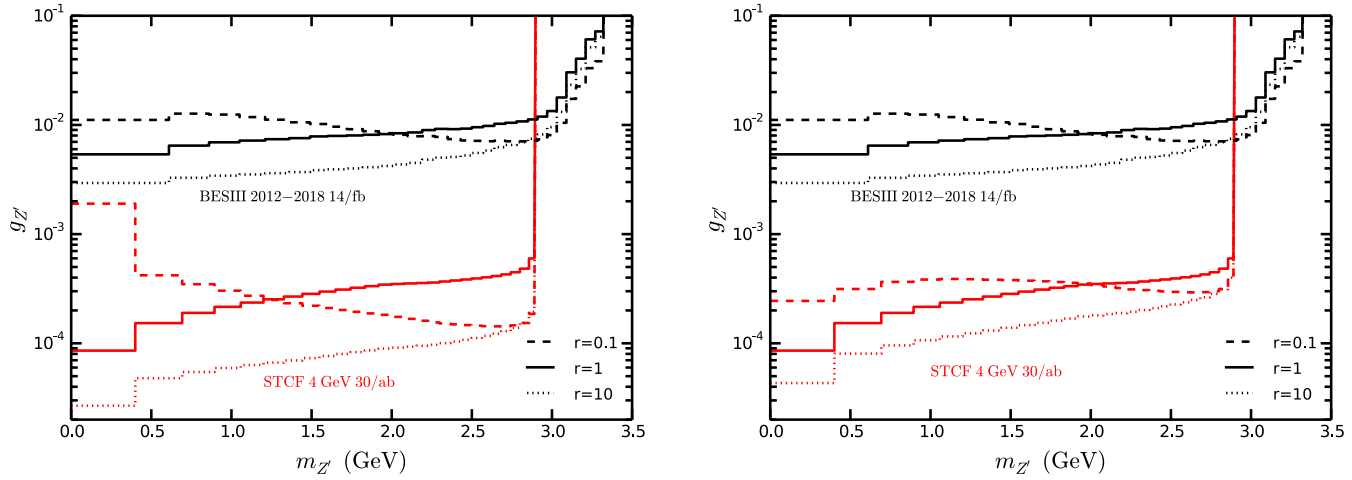

FIG. 8. The expected 95% C.L. exclusion limits on $g_{Z'}$ via monophoton searches after the optimized cut at BESIII with 14 fb^{-1} (black) and 4 GeV STVF with 30 fb^{-1} (red). For the $L_\mu - L_\tau$ model with extra heavy vectorlike leptons (left) or charged scalars (right) in the cases of $r = 0.1$ (dashed), 1 (solid), and 10 (dotted).

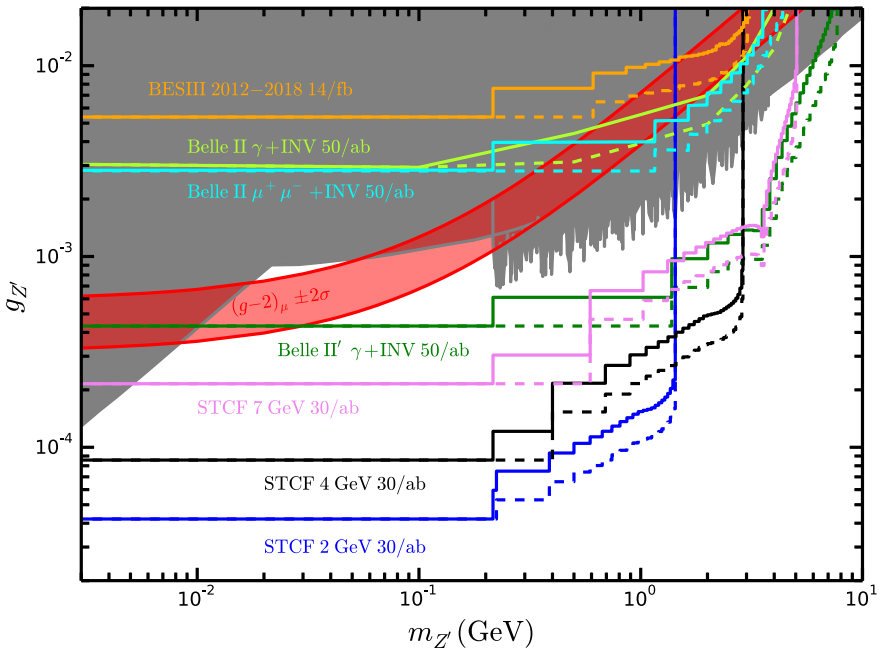

FIG. 9. The sensitivity on gauge coupling $g_{Z'}$ at Belle II, BESIII, and STCF. Notice that we do not include the gBG analysis for BESIII and STCF limits. The solid lines indicate the case in which Z' has no additional decay channel to dark matter, and the dotted lines indicate $\mathrm{Br}(Z' \to \text{invisible}) \simeq 1$ cases. The existing constraints from different experiments are presented in the shaded region and summarized in Fig. 3. The red band shows the region that could explain the muon anomalous magnetic moment $(g-2)_\mu \pm 2\sigma$. The BESIII limit is obtained with the 14 fb^{-1} luminosity of monophoton trigger collected during 2012–2018. The STCF limits are obtained for $\sqrt{s} = 2, 4, 7$ GeV with the future integrated luminosity of 30ab^{-1}. The Belle II limits are obtained with future integrated luminosity of 50ab^{-1} with three experiments (see text for detail).

anomalous magnetic moment $(g-2)_\mu \pm 2\sigma$. We present three expected limits with different experiments at Belle II:

(i) $\gamma + \mathrm{INV}$ *channel with bBG and gBG considered.*—We translate the constraints on the dark photon from the search of invisible decay at Belle II assuming a 20 fb^{-1} dataset [36], where the bBG and gBG are all considered, to the $L_\mu - L_\tau$ gauge boson using the relation of Eq. (15). Then, we scale the constraints to 50 ab^{-1} by a factor of $(\frac{50\ \mathrm{ab}^{-1}}{20\ \mathrm{fb}^{-1}})^{1/4}$. This case is labeled as "Belle II $\gamma + \mathrm{INV}$" in Fig. 9.

(ii) $\gamma + \mathrm{INV}$ *channel with only bBG considered.*—We compute the limits without gBG taken into account as mentioned above. The bBG cuts are applied to remove the reducible BG events, and only the irreducible BG contributes to the BG events if gBG is not considered. After the optimized cut, we show the 95% C.L. upper bound on $g_{Z'}$ at Belle II with the integrated luminosity of 50 ab^{-1} in Fig. 9, which is labeled as "Belle II′$\gamma + \mathrm{INV}$."

(iii) $\mu^+\mu^- + \mathrm{INV}$ *channel.*—To project the sensitivity on the $U(1)_{L_\mu - L_\tau}$ gauge boson Z' with the $e^+e^- \to \mu^+\mu^- Z', Z' \to \mathrm{INV}$ channel in the 50 ab^{-1} Belle II experiment, we simply scale the recent 276 pb^{-1} results by a factor of $(\frac{50\ \mathrm{ab}^{-1}}{276\ \mathrm{pb}^{-1}})^{1/4}$ for the kinetic mixing, which is labeled as "Belle II $\mu^+\mu^- + \mathrm{INV}$."

One observes that on the searches for the invisible decay of Z' the sensitivity at 50 ab^{-1} Belle II with the $\mu^+\mu^- + \mathrm{INV}$ channel is slightly better with the $\gamma + \mathrm{INV}$ channel. It can also be found that these two results are already excluded by current constraints. In the $\gamma + \mathrm{INV}$ channel, if the gBG is not considered, the sensitivity can be improved almost 1 order of magnitude, i.e., $g_{Z'}$ is bounded below to about 4.2×10^{-4} for $m_{Z'} < 2m_\mu$. In this case, we still have a tiny room in the mass region $m \sim (0.01 - 0.03)$ GeV to explain the moun $(g-2)$ anomaly. The 1 order of magnitude difference in sensitivity between the two Belle II limits via the monophoton search shows that the control on gGB is very important in probing the Z' parameter space.

The STCF and BESIII limits are obtained when the BG due to the gaps in the detectors is neglected, since BESIII did not release any analysis about gBG. We emphasize that more rigorous BESIII and STCF sensitivities could be obtained with such gBG analysis available in the future. With about 14 fb^{-1} integrated luminosity collected during 2012–2018 [58], the upper limits from BESIII are excluded by the CCFR experiment. The STCF limits are presented at $\sqrt{s} = 2, (4, 7)$ GeV with the integrated luminosity of 30 ab^{-1}. The future monophoton searches at the STCF experiment operated at $\sqrt{s} = 2$–7 GeV can eliminate the moun $g-2$ favored window when $m_{Z'} \lesssim 5$ GeV. In the low mass region, 2 GeV STCF provides the best sensitivity since the signal to

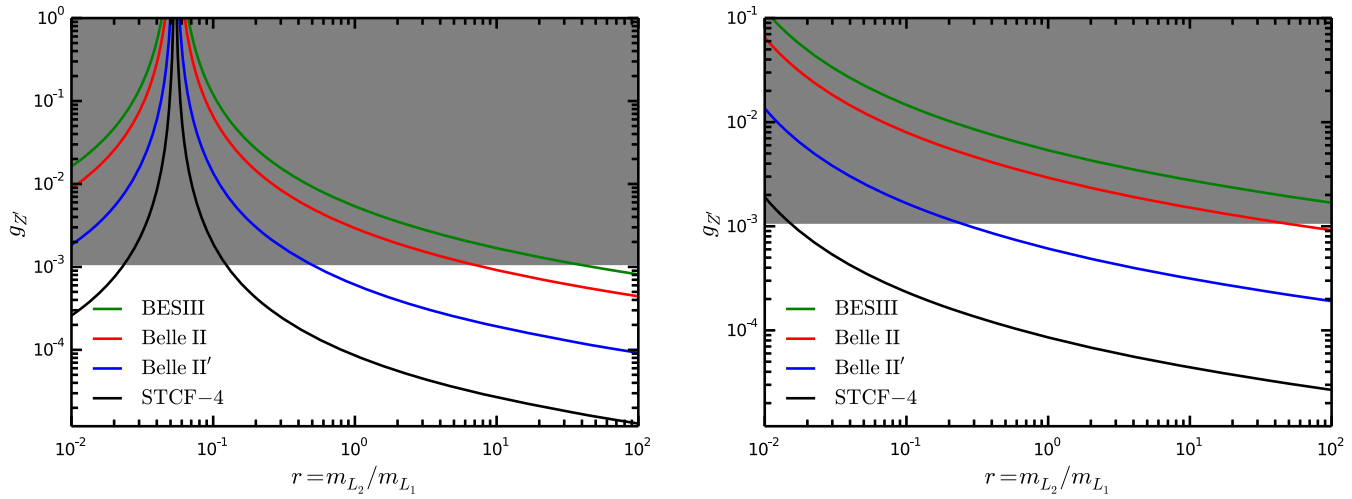

FIG. 10. The expected 95% C.L. exclusion limits in the $g_{Z'}$-r plane for $m_{Z'} = 0.1$ GeV from BESIII with 14 fb^{-1}, Belle II with 50 ab^{-1}, and 4 GeV STCF with 30 ab^{-1}. The shaded gray region is already excluded by CCFR experiments, which is independent on the mass ratio.

BG ratio increases when the colliding energy decreases, and can probe $g_{Z'}$ down to about 4.2×10^{-5} for $m_{Z'} < 2m_\mu$. It can be found that the one order of magnitude increase in sensitivity from 50 ab^{-1} Belle II to STCF could be achieved via monophoton searches when the gBG is omitted.

In Fig. 10, we present the dependence for exclusion regions of $g_{Z'}$ corresponding to $m_{Z'} = 0.1$ GeV on the mass ratio $r = m_{L_2}/m_{L_1}$ and $r = m_{S_2}/m_{S_1}$ via monophoton searches from BESIII with 14 fb^{-1}, Belle II with 50 ab^{-1}, and future 4 GeV STCF with 30 ab^{-1}. The shaded gray region is already excluded by CCFR experiments, which is independent of the mass ratio. One can see that $g_{Z'}$ can go down to $1.3(2.7) \times 10^{-5}$ when $m_{L_2}/m_{L_1}(m_{S_2}/m_{S_1}) = 100$ at 4 GeV STCF with 30 ab^{-1}.

VIII. SUMMARY

In this paper, we probe the invisible decay of the $L_\mu - L_\tau$ gauge boson via monophoton signature at three different electron colliders operated at the GeV scale: Belle II, BESIII, and STCF. In the minimal $U(1)_{L_\mu - L_\tau}$ model, we extend the SM with a $U(1)_{L_\mu - L_\tau}$ gauge symmetry and assume that the kinetic mixing term between Z' and photon is absent at tree level but can arise at one-loop level due to μ and τ leptons. We also further extend the minimal $U(1)_{L_\mu - L_\tau}$ model with extra heavy vectorlike leptons or charged scalars, where the additional contributions to the kinetic mixing arising from extra particles inside the loop. The exciting nondecoupling behavior of the contribution from the extra heavy vectorlike leptons or charged scalars to the kinetic mixing is also demonstrated. The visible signatures of heavy leptons or charged scalars, too heavy to be directly detected at high-energy colliders, may be possible in processes modified by the $\gamma - Z'$ mixing.

We translate the sensitivity for dark photon within the monophoton signature projected by Belle II to the $U(1)_{L_\mu - L_\tau}$ gauge boson taking into account various SM BGs. We also recast the recent invisible search of Z' in the $\mu^+\mu^- Z'$ production at Belle II. It is found that, by ignoring the BG due to the gaps in the detectors, we present the constraints at BESIII with 14 fb^{-1} luminosity and at future 30 ab^{-1} STCF. For comparison, we also compute the limits at 50 ab^{-1} Belle II without gBG taken into account. It is found that the future 2 GeV STCF can further improve the sensitivity to low mass Z' than Belle II via the monophoton signature since it is operated at lower energy. The future STCF can exclude the moun $g-2$ anomaly favored parameter region when $m_{Z'} \lesssim 5$ GeV. And the gauge coupling constant $g_{Z'}$ in the minimal $U(1)_{L_\mu - L_\tau}$ model can be probed down to about 4.2×10^{-5} when $m_{Z'} < 2m_\mu$ at future 30 ab^{-1} STCF with $\sqrt{s} = 2$ GeV.

ACKNOWLEDGMENTS

This work was supported in part by the National Natural Science Foundation of China (Grants No. 11805001 and No. 11935001).

[1] R. Foot, Mod. Phys. Lett. A **06**, 527 (1991).
[2] X. He, G. C. Joshi, H. Lew, and R. Volkas, Phys. Rev. D **43**, R22 (1991).
[3] X. He, G. C. Joshi, H. Lew, and R. Volkas, Phys. Rev. D **44**, 2118 (1991).
[4] G. W. Bennett *et al.* (Muon g-2 Collaboration), Phys. Rev. D **73**, 072003 (2006).
[5] S. Baek, N. G. Deshpande, X. G. He, and P. Ko, Phys. Rev. D **64**, 055006 (2001).
[6] E. Ma, D. P. Roy, and S. Roy, Phys. Lett. B **525**, 101 (2002).
[7] W. Altmannshofer, C. Y. Chen, P. S. Bhupal Dev, and A. Soni, Phys. Lett. B **762**, 389 (2016).
[8] R. Aaij *et al.* (LHCb Collaboration), Phys. Rev. Lett. **111**, 191801 (2013).
[9] R. Aaij *et al.* (LHCb Collaboration), Phys. Rev. Lett. **113**, 151601 (2014).
[10] W. Altmannshofer, S. Gori, S. Profumo, and F. S. Queiroz, J. High Energy Phys. 12 (2016) 106.
[11] A. Crivellin, G. D'Ambrosio, and J. Heeck, Phys. Rev. Lett. **114**, 151801 (2015).
[12] P. Ko, T. Nomura, and H. Okada, Phys. Rev. D **95**, 111701 (2017).
[13] S. Baek, Phys. Lett. B **781**, 376 (2018).
[14] Y. Jho, S. M. Lee, S. C. Park, Y. Park, and P. Y. Tseng, J. High Energy Phys. 04 (2020) 086.
[15] W. Altmannshofer, M. Carena, and A. Crivellin, Phys. Rev. D **94**, 095026 (2016).
[16] S. Baek, H. Okada, and K. Yagyu, J. High Energy Phys. 04 (2015) 049.
[17] J. Heeck and W. Rodejohann, Phys. Rev. D **84**, 075007 (2011).
[18] A. Biswas, S. Choubey, and S. Khan, J. High Energy Phys. 09 (2016) 147.
[19] S. Patra, S. Rao, N. Sahoo, and N. Sahu, Nucl. Phys. **B917**, 317 (2017).
[20] A. Biswas, S. Choubey, and S. Khan, J. High Energy Phys. 02 (2017) 123.
[21] A. Biswas, S. Choubey, L. Covi, and S. Khan, J. Cosmol. Astropart. Phys. 02 (2018) 002.
[22] G. Arcadi, T. Hugle, and F. S. Queiroz, Phys. Lett. B **784**, 151 (2018).
[23] A. Kamada, K. Kaneta, K. Yanagi, and H. B. Yu, J. High Energy Phys. 06 (2018) 117.
[24] P. Foldenauer, Phys. Rev. D **99**, 035007 (2019).
[25] Y. Cai and A. Spray, J. High Energy Phys. 10 (2018) 075.
[26] Z. L. Han, R. Ding, S. J. Lin, and B. Zhu, Eur. Phys. J. C **79**, 1007 (2019).
[27] J. P. Lees *et al.* (*BABAR* Collaboration), Phys. Rev. D **94**, 011102 (2016).
[28] I. Adachi *et al.* (Belle II Collaboration), Phys. Rev. Lett. **124**, 141801 (2020).
[29] A. M. Sirunyan *et al.* (CMS Collaboration), Phys. Lett. B **792**, 345 (2019).
[30] Y. Jho, Y. Kwon, S. C. Park, and P. Y. Tseng, J. High Energy Phys. 10 (2019) 168.
[31] Y. Kaneta and T. Shimomura, Prog. Theor. Exp. Phys. (**2017**), 053B04.
[32] T. Araki, S. Hoshino, T. Ota, J. Sato, and T. Shimomura, Phys. Rev. D **95**, 055006 (2017).
[33] C. H. Chen and T. Nomura, Phys. Rev. D **96**, 095023 (2017).
[34] H. Banerjee and S. Roy, Phys. Rev. D **99**, 035035 (2019).
[35] G. Krnjaic, G. Marques-Tavares, D. Redigolo, and K. Tobioka, Phys. Rev. Lett. **124**, 041802 (2020).
[36] E. Kou *et al.* (Belle II Collaboration), Prog. Theor. Exp. Phys. (**2019**), 123C01; (**2020**), 029201(E).
[37] D. M. Asner *et al.*, Int. J. Mod. Phys. A **24**, S1 (2009).
[38] A. E. Bondar *et al.* (Charm-Tau Factory Collaboration), Yad. Fiz. **76**, 1132 (2013).
[39] Q. Luo and D. Xu, *Proceedings of the IPAC2018, Vancouver, BC, Canada* (JACoW Publishing, Geneva, Switzerland, 2018).
[40] H. Peng, https://indico.inp.nsk.su/event/15/session/0/contribution/99/material/slides/0.pdf.
[41] M. Tanabashi *et al.* (Particle Data Group), Phys. Rev. D **98**, 030001 (2018).
[42] W. Altmannshofer, S. Gori, M. Pospelov, and I. Yavin, Phys. Rev. Lett. **113**, 091801 (2014).
[43] G. Magill and R. Plestid, Phys. Rev. D **95**, 073004 (2017).
[44] M. Bauer, P. Foldenauer, and J. Jaeckel, J. High Energy Phys. 07 (20180) 094.
[45] D. W. P. do Amaral, D. G. Cerdeno, P. Foldenauer, and E. Reid, arXiv:2006.11225.
[46] R. Harnik, J. Kopp, and P. A. N. Machado, J. Cosmol. Astropart. Phys. 07 (2012) 026.
[47] G. Bellini *et al.*, Phys. Rev. Lett. **107**, 141302 (2011).
[48] M. Abdullah, J. B. Dent, B. Dutta, G. L. Kane, S. Liao, and L. E. Strigari, Phys. Rev. D **98**, 015005 (2018).
[49] M. Agostini *et al.* (Borexino Collaboration), Phys. Rev. D **100**, 082004 (2019).
[50] J. Lees *et al.* (*BABAR* Collaboration), Phys. Rev. Lett. **119**, 131804 (2017).
[51] R. Essig, P. Schuster, and N. Toro, Phys. Rev. D **80**, 015003 (2009).
[52] J. Liang, Z. Liu, Y. Ma, and Y. Zhang, Phys. Rev. D **102**, 015002 (2020).
[53] P. F. Yin, J. Liu, and S. H. Zhu, Phys. Lett. B **679**, 362 (2009).
[54] M. Ablikim *et al.* (BESIII Collaboration), Phys. Rev. D **96**, 112008 (2017).
[55] Z. Liu, Y. H. Xu, and Y. Zhang, J. High Energy Phys. 06 (2019) 009.
[56] Z. Liu and Y. Zhang, Phys. Rev. D **99**, 015004 (2019).
[57] M. Ablikim *et al.* (BESIII Collaboration), Phys. Rev. D **83**, 112005 (2011).
[58] Y. Zhang, W. T. Zhang, M. Song, X. A. Pan, Z. M. Niu, and G. Li, Phys. Rev. D **100**, 115016 (2019).